AD-A110 525 STANFORD UNIV CA EDWARD L GINZTON LAB OF PHYSICS F/G 20/1
RESEARCH ON NONDESTRUCTIVE TESTING.(U)
NOV 81 G S KINO F49620-79-C-0217
UNCLASSIFIED GL-3363 AFOSR-TR-82-0030 NL

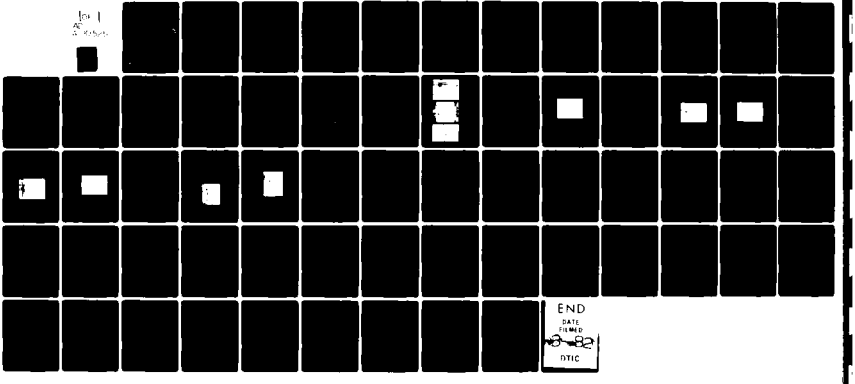

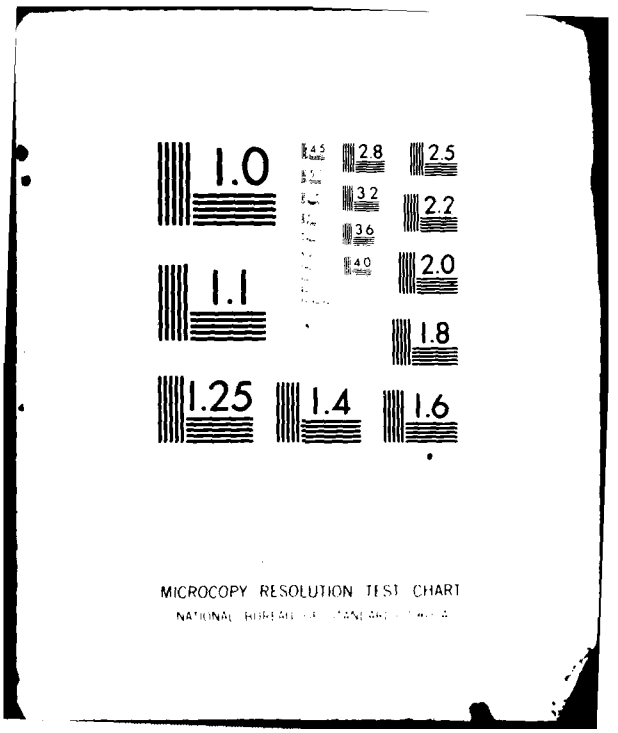
1.0
1.1
1.25
1.4
1.6
1.8
2.0
2.2
2.5
2.8
3.2
3.6
4.0
MICROCOPY RESOLUTION TEST CHART

LEVEL II

(10)

YEAR END REPORT

RESEARCH ON NONDESTRUCTIVE TESTING

for

Air Force Office of Scientific Research

Contract No. F49620-79-C-0217

for the period

September 1, 1980 - August 31, 1981

NOVEMBER 1981

G. L. Report No. 3363

Principal Investigator: G. S. Kino

Edward L. Ginzton Laboratory
W. W. Hansen Laboratories of Physics
Stanford University
Stanford, California 94305

AIR FORCE OFFICE OF SCIENTIFIC RESEARCH (AFSC)
NOTICE OF TRANSMITTAL TO DTIC
This technical report has been reviewed and is
approved for public release IAW AFR 190-12.
Distribution is unlimited.
MATTHEW J. KERPER
Chief, Technical Information Division

TABLE OF CONTENTS

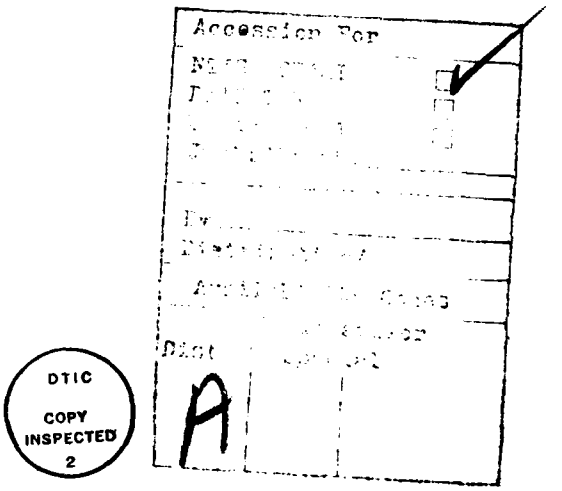

I. INTRODUCTION

Good progress has been made in the last year on a number of different fronts. Our aim has been to develop more rapid methods of NDE, as well as quantitative techniques for determining the parameters such as stress and microstructure associated with different types of materials, in particular steels.

The imaging work has made a great deal of progress. The digital imaging system is now working well. We have used a number of different modes of propagation to make quantitative observations of cracks. We have developed special-purpose transducer arrays, for instance, a contacting shear wave array, a contacting longitudinal wave array, and array systems suitable for pitch/catch operation. Operating at a center frequency of 3.3 MHz , we have demonstrated that we can observe extremely small cracks with a size as small as 1 mm, located on the opposite side of a metal sample being examined, and can size these cracks. We have demonstrated that by carrying out additional processing of the original real-time images using the computer, we can improve the quality of the image and obtain further quantitative information. The nature of the sidelobes is now well-understood and we have succeeded in decreasing the amplitude of the sidelobes due to digital sampling by orders of magnitude.

New collocation theoretical techniques have been developed for determining the stress field around a crack in a semi-infinite half-space. These have proven extremely useful to the rest of our program as an input on which to check experiments and other theoretical techniques. They are also of

fundamental importance to the theory of scattering of acoustic waves from cracks.

A great deal of work has been done on microstructural measurements. These are of importance for determining hardness, fracture toughness and other characteristics of materials. We have used attenuation techniques, velocity measurement techniques with bulk waves and surface waves for determining near-surface microstructure, and we have developed new theoretical methods for this purpose. We have developed and are developing various types of tools for associating our acoustic measurements with the microstructural properties of materials.

The work on energy integrals has made good progress. The importance of this work is that it may, in the end, lead to insight into the crack skewing phenomenon when a crack grows under applied stresses. Energy integrals associated with a crack have been measured by acousto-elastic techniques, and we are trying to develop further methods using shear waves to obtain more experimental information on the various types of energy integrals.

A new fiber-optic probe for measuring the amplitude and phase of acoustic waves excited on a metal surface has been developed. The aim of this work is to make a non-contacting acoustic probe. A fiber-optic link makes it possible to obtain definitions of 4-6 μm with the optical equipment located on a bench remote from the sample being tested.

II. ACOUSTIC IMAGING

S. D. Bennett, K. Peterson, A. Selfridge

1. Introduction

The real-time imaging hardware operating at a center frequency of 3.3 MHz is fully debugged and operational. We now have an extensive library of software which both emulates the hardware and extends its capabilities. In conjunction, the hardware and associated computer programs are a powerful tool in the analysis of the NDE acoustic imaging process. Real-time hardware allows us to experiment with many different imaging parameters at once; their consequences are immediately seen on the display screen. Ancillary computer programs allow us to manipulate this data to suppress certain aberrations and to experiment with different reconstruction algorithms.

In a digital imaging system, quantization errors are a possible source of image degradation. The amplitude quantization (8 bits/sample) does not appear to be an immediate problem. However, the quantization in the time domain leads to sidelobes which are both broader in extent and larger in amplitude than desired. The results of Section 2 suggest that interpolation of the echo data before reconstruction decreases the sidelobe level. The decrease in sidelobe level would come at a cost of greater imaging hardware complexity. A much simpler solution would be to increase the basic sampling rate of the imaging system so that we would have perhaps five samples per wavelength instead of three. With the same amount of memory, this would lead to a smaller field of view, since the number of pixels in the reconstructed field is constant.

The reconstruction algorithm is directed by firmware in the imaging system.[1,2] This allows us some latitude in the geometry of the transmitter and receiver sections. Section 3 presents results of a pitch/catch imaging experiment in which a surface flaw was illuminated from the back side and an image was reconstructed from the scattered waves.[4,5] This method shows great promise for imaging crack features such as crack depth.

In Section 4 we present images collected with new types of direct contacting arrays, which launch either longitudinal, Rayleigh or shear waves in aluminum.[3,4,5] These arrays are simple to use, requiring only a thin smear of water or gel as a coupling medium. The direct contacting shear wave array is a particularly important breakthrough because the slower velocity of shear waves gives a factor of two improvement in lateral resolution compared to a similar longitudinal array. Shear waves are best for interrogating cracks and because of the use of an angled buffer rod. Reflections from large surfaces, such as the front and back faces of the sample, are eliminated.

Finally, in Section 5, we describe a feasibility experiment to show that a large aperture system can be synthesized by compound scanning. The intensities of several images are obtained from different angles of incidence. This makes it possible to observe highly curved flaws and to reduce considerably the sidelobe levels, grain scattering, noise, and speckle effects which tend to occur in acoustic images.

2. Time Quantization Errors

The figures in this section are contour plots of a simulated line target perpendicsiar to the imaging plane at a range of 80 mm in water. The aperture is 16 mm wide and the imaging pulse is a Gaussian envelope cosine wave with two rf cycles between 1/e points and a center frequency of 3.5 MHz . The first contour level is at -3 dB and the other contours are at multiples of -6 dB (i.e., -3, -6, -12, -18, -24,..). Figure II.1a shows the reconstruction of the simulated line target using a computer based algorithm which exactly mimics the imaging hardware when it is running at a 10.5 MHz sampling rate (three samples per center frequency wavelength). The main lobe has approximately the same shape as we expect, but the sidelobes are larger and extend far away from the main lobe. From a simple theory,[1] we would expect the first sidelobe to be -19 dB down, but it is only -14 dB down. Our theoretical studies lead us to believe that the high sidelobes might be due to quantization errors introduced by the digital nature of the stored echo data.

Since the data collected by the imaging system is sampled at above the Nyquist rate, it is possible to interpolate the echo data to remove the time quantization error. Figure II.1b shows the reconstruction of the same line target using interpolated data. Now the first sidelobe is about -19 dB , in good agreement with theory. The far out sidelobes are down at the -40 dB level. The point spread function shown in Figure II.1b has a distinct "bow-tie" shape with higher sidelobe levels on the perimeter and lower levels on the interior. With interpolation, the signals back-projected into the interior of the bow-tie overlap with each other and destructively interfere.

When the back-projected signals are not interpolated, they contain many large discontinuities which lead to incomplete cancellation so that the sidelobe levels are higher in the interior of the uninterpolated point spread function. The signals backprojected near the perimeter of the bow-tie correspond to the transducer elements near the ends of the array. Since the array aperture truncates abruptly at the ends, we observe a Gibb's ringing phenomenon near the perimeter of the point spread function. We would expect that by apodizing the aperture, that is, weighting the central elements more heavily than the end elements of the array, the ringing would be reduced. This is analogous to the use of windowing functions in FIR digital filters.[3]

Figure II.1c shows the same line target reconstructed using interpolation and Hanning aperture apodization. As predicted, the ringing at the perimeter of the bow-tie has been substantially reduced so that the far out sidelobes are now well below the -40 dB level. The compactness of the sidelobe structure has been gained at the expense of a wider main lobe (1.6 mm versus 1.0 mm for the unapodized array).

The above results show that computer based reconstructions can be expected to improve the images significantly. We offer one typical example here. Figure II.2 shows a shear wave array directly bonded to an aluminum sample with four saw cuts, three straight slots perpendicular to the imaging plane, and one circular arc in the imaging plane. The wavelength in this example is about 1 mm so that the shallowest slot is quite challenging to image (wavelength ~1 mm). Figure II.3a shows an image obtained with the input amplifier gain turned down so that the only significant feature is the reflection from the back wall of the sample. When the amplifier gain is

turned up, we observe the image in Figure II.3b. The image of the back wall is smeared out, but the images of the four cuts are now visible, althougn the 1 mm deep slot is quite faint. Only that portion of the circular arc which faces the array is visible, since the saw cut acts as a specular reflector. Figure II.3c shows the same echo data reconstructed using interpolation. Three improvements are evident here. First, the image of the shallow 1 mm slot stands out better. We can even see the "shadow" of the slot in the backface reflection. Second, the images of the slots are more compact in the lateral dimension due to a more compact sidelobe structure. Finally, the backface reflection is smoother; it doesn't have the hispid appearance of Figures II.3a and II.3b. This is because reconstructing with interpolation generates smaller, more compact sidelobes which give less interference fringing in the reconstruction of extended objects such as specular reflectors.

3. Separation of Transmitter and Receiver--Pitch/Catch Imaging

We have previously shown[1,2] images of slots and surface cracks obtained with an edge-bonded surface wave array. In these images the locations of the flaws with respect to the array were easily obtained. However, there was no method for determining the depth or structure of the crack. In this section we describe experiments in which we separate the transmitting and receiving functions of the imaging system so that we may illuminate a flaw from one angle while observing the waves scattered off at a different angle. A typical pitch/catch experiment is shown in Fig. II.4. A 19 mm diameter longitudinal wave transducer is used to illuminate the crack from above and an image is

formed from the scattered waves which reach the receiving Rayleigh wave array. This imaging geometry suffers a factor of two loss in lateral resolution compared to the normal pulse/echo geometry because the target must move laterally twice as far to give the same phase change across the array. However, this disadvantage is more than offset by the increased information we can gather about the crack using the pitch/catch geometry.

The first sample we looked at was a 7 mm deep x .5 mm wide slot, milled in an aluminum block. Figure II.5 shows the image obtained with this sample. We observe not one but three multiple images of the crack followed by other less distinct features. The full extent of the slot is not visible since the illuminating transducer is only about one third as wide as the image field. We believe that the first three stripes are due to three different scattered waves coming from different portions of the slot, while the other poorly focused features are due to multiple reflections off the faces and edges of the aluminum block.

Figure II.6 is a schematic description of the three types of waves scattered from different portions of the slot. The fastest is a shear wave which scatters from the crack tip and travels a glancing trajectory toward the plastic coupling strip. This wave arrives first and reconstructs as the left-most stripe in Fig. II.5, where it couples into a Rayleigh wave on the array substrate. The next fastest wave is a Rayleigh wave which scatters off the crack opening. This reconstructs as the middle bright bar in Fig. II.5. The slowest wave is one which scatters into a Rayleigh mode at the crack tip, travels down the crack face, and then turns a right angle and continues as a Rayleigh wave along the horizontal surface of the sample. This wave travels

the slowest and longest route and therefore reconstructs as the third bright bar in Fig. II.5. The difference in arrival times of these three waves is shown in Fig. II.6. By measuring these arrival times, or alternatively by measuring their displacements in the image, we can infer the depth of the crack.

Since there is only one unknown (the depth of the crack, h) and there are two independent arrival time intervals (say Δt_1 and Δt_2), we have two different ways to measure the crack depth. In this experiment we predict a crack depth of 7.5 mm based on the measurement of Δt_2 and 5.5 mm based on the mesurement of Δt_1. Since the Rayleigh and shear wave velocities are nearly the same, crack depth predictions based on Δt_1 are inherently less reliable than those based on Δt_2.

Next, we used the same technique to look at a real 10 mm wide fatigue crack, shown in Fig. II.7. The surface breaking portion of the crack is uneven and has a prominent bend in it about one third of the way across. Cracks of this sort should normally be about 4 mm deep, but the uneven surface may cause it to behave more like two adjacent but smaller cracks. An image of the crack, using the pitch/catch geometry, with the illuminating transducer directly overhead, is shown in Fig. II.8. The shear wave mode seems to be absent. The first bright bar is the surface wave mode scattered by the crack opening. This is followed immediately by a fainter bar which is due to Rayleigh waves scattered from the crack tip. The bend in the crack occurs about one third of the way down from the top of the bright bar. The secondary echo is fainter here, perhaps indicating that the crack is not so deep, or perhaps bent off in a different direction. The position of the

second echo indicates an average depth of 3 to 4 mm , in agreement with our expectations.

4. Imaging With Direct Contacting Arrays

Still another way of looking at flaws for NDT applications is with bulk waves. In this section we describe images of the same fatigue crack made with both longitudinal and shear wave arrays. A special feature of these arrays is that they operate in direct contact with the sample being examined. Both arrays use a flat, lapped contacting surface with a thin layer of coupling fluid (usually water or Sonotrac coupling gel). The samples are easily moved over the array for best positioning of the flaw.

Figure II.9 shows an experiment in which we examine the 10 mm fatigue crack at an oblique angle with the contacting longitudinal wave array. The image obtained is shown in Figure II.10. The crack is the first bright feature to the right of the array (increasing range is to the right). The image is heavily cluttered behind the crack due to multipath reflections off the many facets of the angle block and sample.

Figure II.11 shows an image of the same fatigue crack made with a new contacting shear wave array we have constructed for this work. This is constructed on a metal block cut at 45° to the angle of incidence.[4] The image is much clearer because the array is constructed directly on a large angle block, so there are not many paths for multiple reflections. Making contact is very easy with this array because the angle block is cut at 45° . This makes it simple to transmit shear waves across the contact region. A series of bars behind the primary image of the crack may be due to

acoustic energy trapped in the crack and bouncing back and forth between the crack tip and crack opening, slowly leaking out. The period of oscillation of these trailing echoes may be indicative of the depth of the crack. Also in the picture we see the effect of the sharp jog in the crack. Here the jog appears one third of the way from the bottom of the crack image since we are looking at the crack from the back side, as compared with Figs. II.4 and II.8. We believe that, because of the simplicity of its use, this new direct contacting shear wave array is an important advance in the state of the art in NDE acoustic imaging.

5. Compound Scanning

The linear array system has two main limitations due to its format: (1) sidelobes due to the use of a finite number of transducer array elements (32); and (2) the fact that we can only observe specular reflectors over a limited range of angles.

One approach to this problem is to scan the transducer array mechanically in a circular path centered on the center of the field of view. In this way, a composite picture can be obtained over a wide angular range. By adopting this procedure, one should obtain a definition at least as good as the original focused imaging system. The main lobes from any particular point should coincide, while the sidelobes will not coincide with each other. Consequently, the ratio of the main lobe to sidelobe level is increased and the results are very much like those to be expected from an incoherent imaging system. Furthermore, it is possible by this procedure to image specular reflectors over a wider range of angles.

A simple example of this compound scanning procedure is shown in Fig. II.12. The aim was to image a cylindrical hole, using surface acoustic waves at a center frequency of 3.3 MHz . A picture of this hole, taken from a single viewing angle, is shown in Fig. II.13. Several pictures were taken from different angles, and by using fiduciary marks to obtain accurate locations, the pictures were superimposed upon each other photographically (see Fig. II.14). The circular shape of the hole shows up clearly and the effective sidelobe levels are considerably decreased, thus forming a far better quality image. We suggest that this procedure could, in fact, be adopted in practice by supporting the array from a mechanical medical B-scan system of high accuracy. As is done with medical B-scan, a picture could be painted of the region of interest. In this case, however, the individual pictures which contribute to the final image would themselves be dynamically focused images, thus improving the definition.

Using an unfocused system, Gebhardt et al[6] demonstrated such a procedure with an NDT application with a rectilinear mechanically-scanned electronic radial sector scan system. The improvement here is that we use a focused beam.

References

1. G. S. Kino, D. Corl, S. Bennett, and K. Peterson, "Real-Time Synthetic Aperture Imaging System," Proceedings of IEEE Ultrasonics Symposium, Boston, Mass., November, 1980.

2. S. Bennett, D. K. Peterson, D. Corl, and G. S. Kino, "A Real-Time Synthetic Aperture Digital Acoustic Imaging System," Proceedings of the Tenth International Acoustic Imaging Conference, Cannes, France, October, 1980, Plenum Press.

3. R. Baer. A. R. Selfridge, B. T. Khuri-Yakub, and G. S. Kino, "Contacting Transducers and Transducer Arrays for NDE," Proceedings of the IEEE Ultrasonics Symposium, Chicago, Ill., October, 1981; to be published.

4. D. K. Peterson, R. Baer, K. Liang, S. D. Bennett, B. T. Khuri-Yakub, and G. S. Kino, "Quantitative Evaluation of Real-Time Synthetic Aperture Acoustic Images," Presented at the DARPA/AFML Review of Progress in Quantitative NDE, Boulder,Colorado, August, 1981.

5. D. K. Peterson, S. D. Bennett, and G. S. Kino, "Real-Time Imaging," Presented at the 1981 Ultrasonics Symposium, Chicago, Illinois, October, 1981.

6. W. Gebhardt, F. Bonitz, H. Woll, and V. Schmitz, "Determination of Crack Characteristics, Size and Orientation of Defects by Phased Array Techniques in NDT," Third International Conference on Nondestructive Evaluation in the Nuclear Industry, Salt Lake City, Utah, February, 1980.

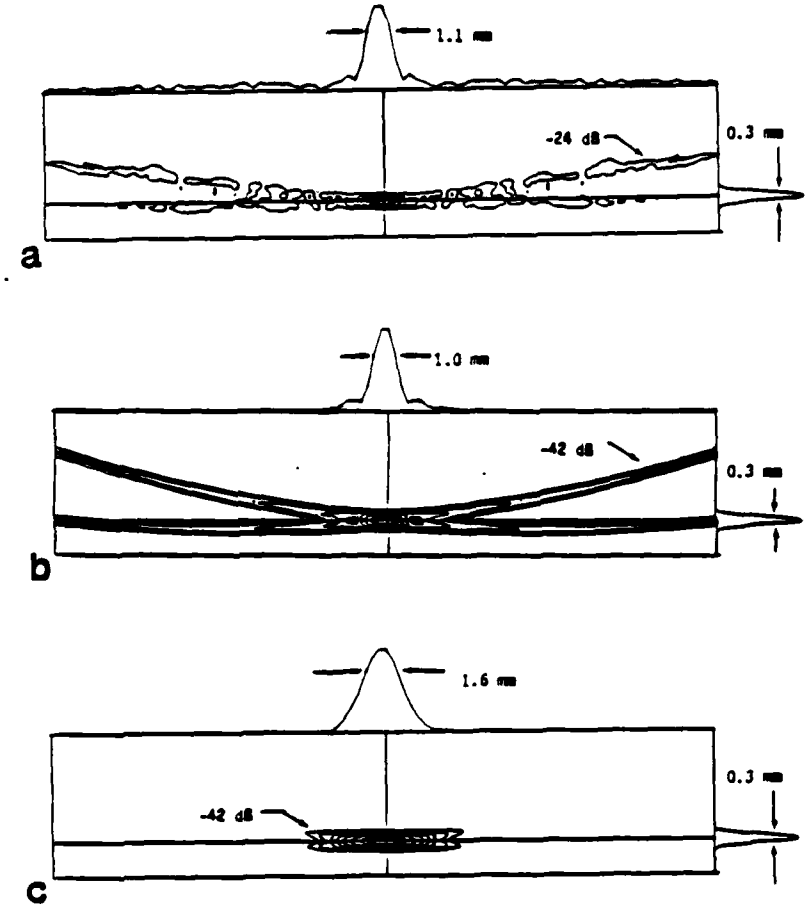

Fig. II.1. (a) Contour plot of reconstructed line reflector using three digital samples per wavelength; (b) contour plot of reconstructed line reflector using continuous sampling of phase; and (c) contour plot of reconstructed line reflector using continuous phase sampling and Hanning aperture apodization.

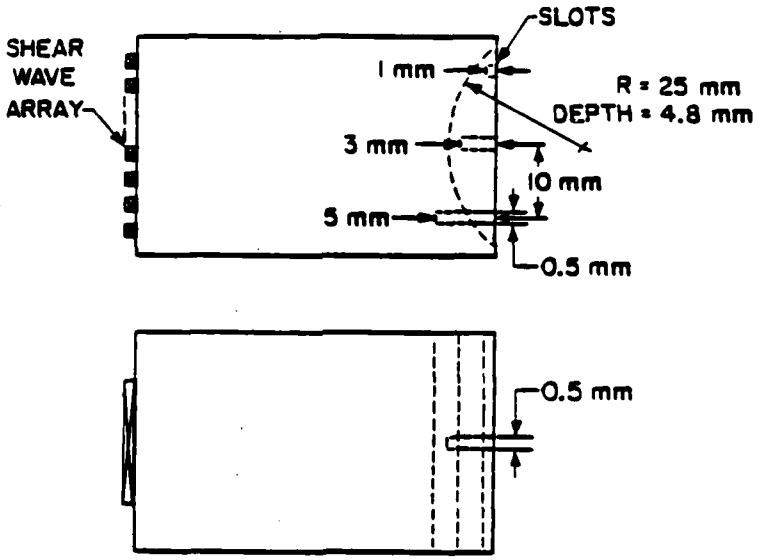

Fig. II.2. Shear wave array directly bonded to a sample with four saw cuts.

Fig. II.3.

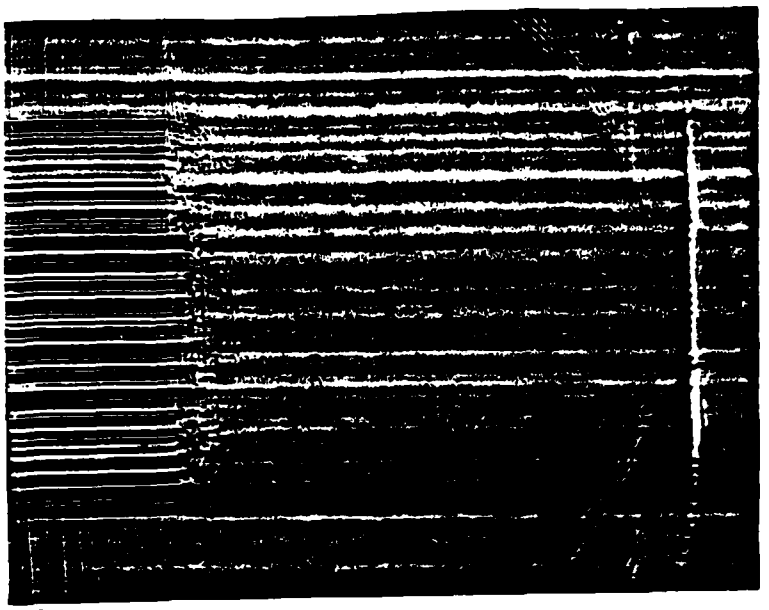

a

Image of sample shown in Fig. II.2. with input amplifier gain turned down. Only the back wall of the sample is visible here.

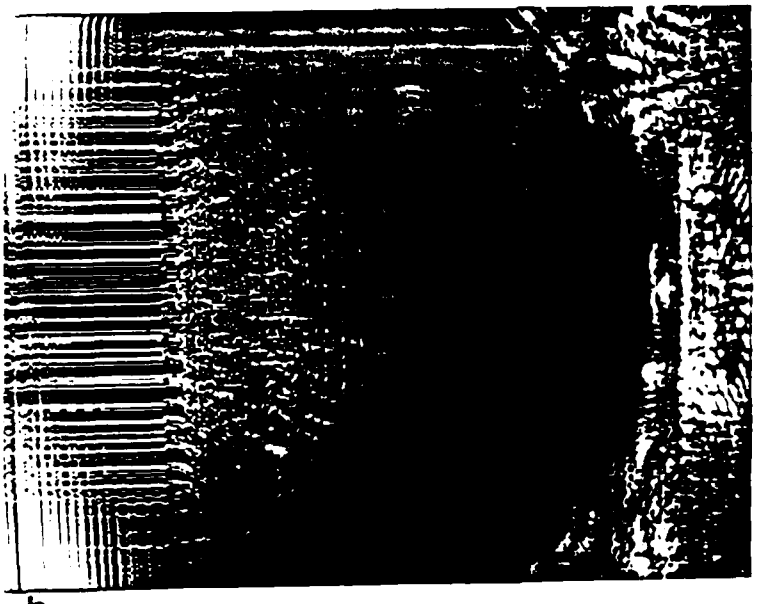

b

With the amplifier gain turned up, the four saw cuts are visible.

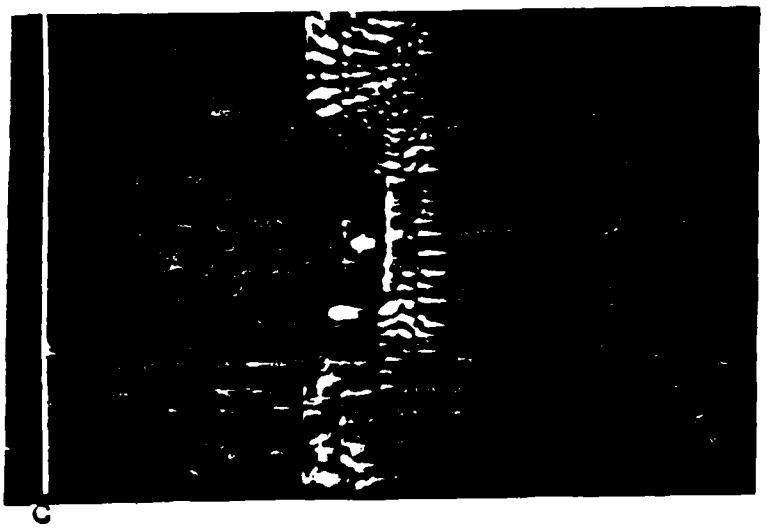

c

A selected portion of (b) reconstructed with continuous interpolation of the discrete echo data. The images of the flaws are now more compact and the shallow (1 mm) slot is well differentiated from the back wall.

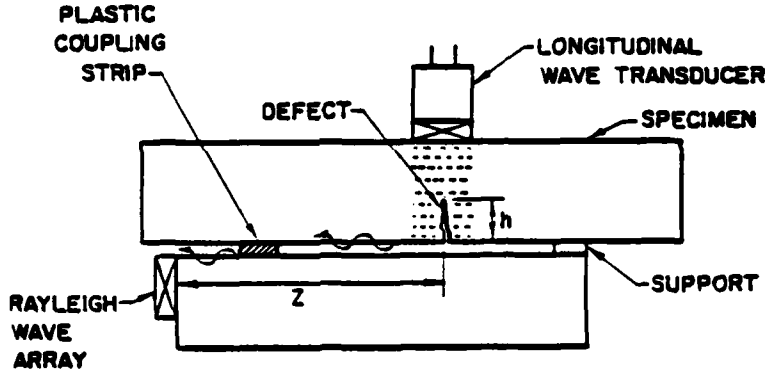

Fig. II.4. Schematic diagram of the transmitter/receiver geometry used in the pitch/catch imaging experiments.

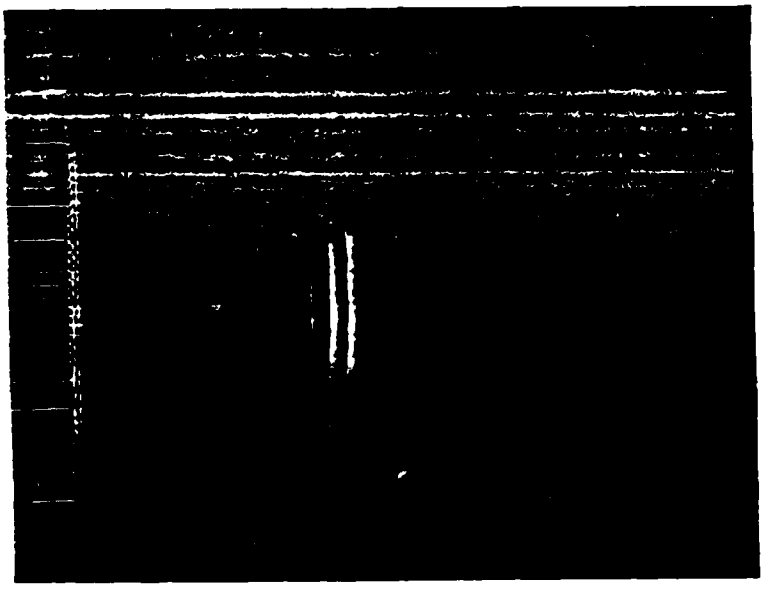

Fig. II.5. Pitch/catch image of a 7 mm deep slot showing three distinct waves scattered from the flaw.

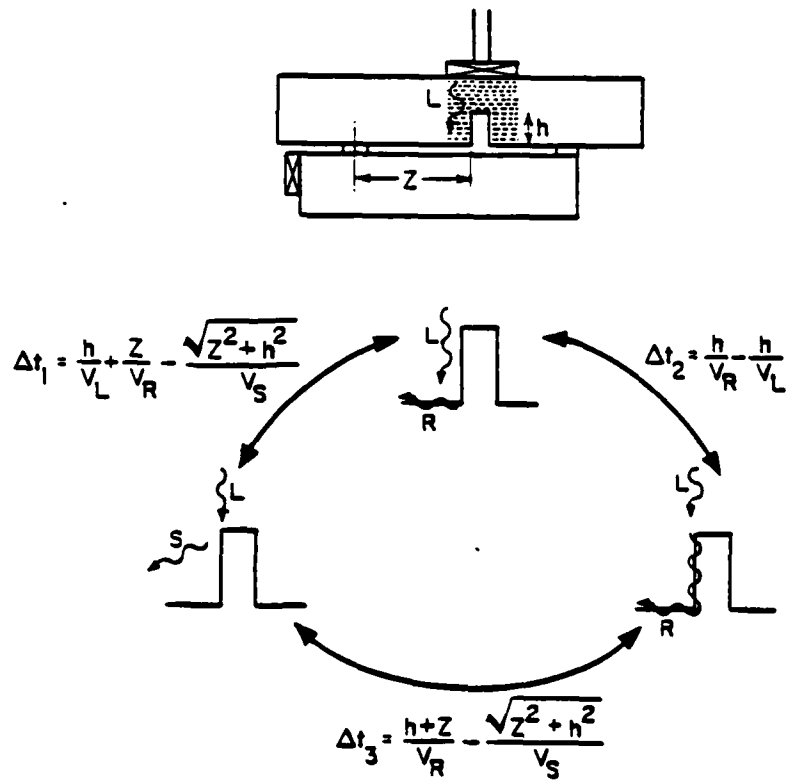

Fig. II.6. Three waves are scattered from the flaw: a shear wave from the crack tip, a Rayleigh wave from the crack opening, and a Rayleigh wave from the crack tip.

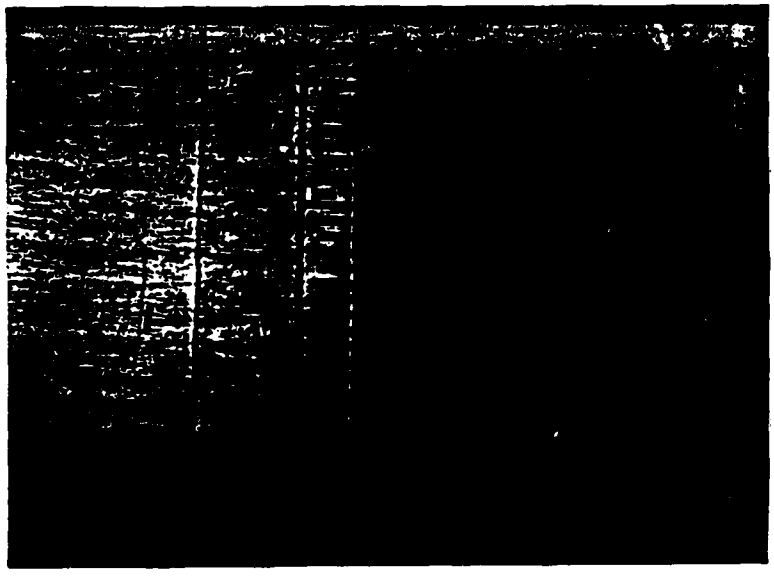

Fig. II.7. Photograph of the 10 mm fatigue crack showing the irregular path of the crack along the surface.

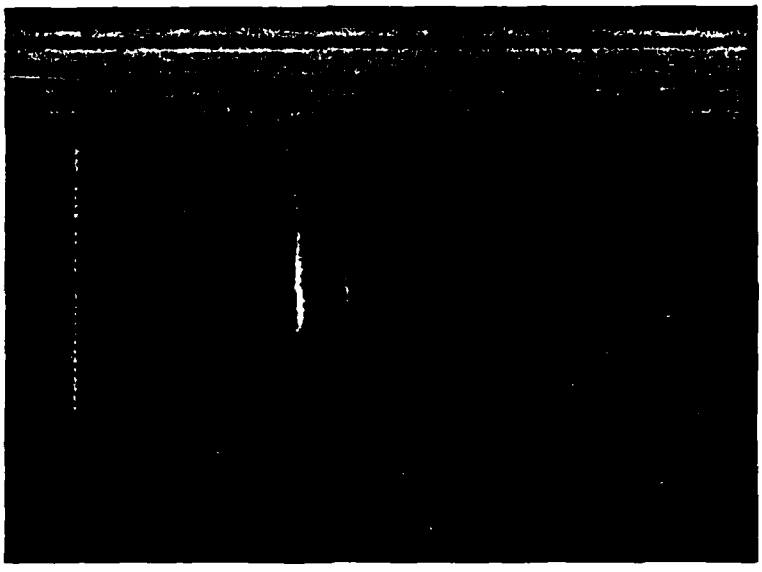

Fig. II.8. Pitch/catch image of the 10 mm wide fatigue crack.

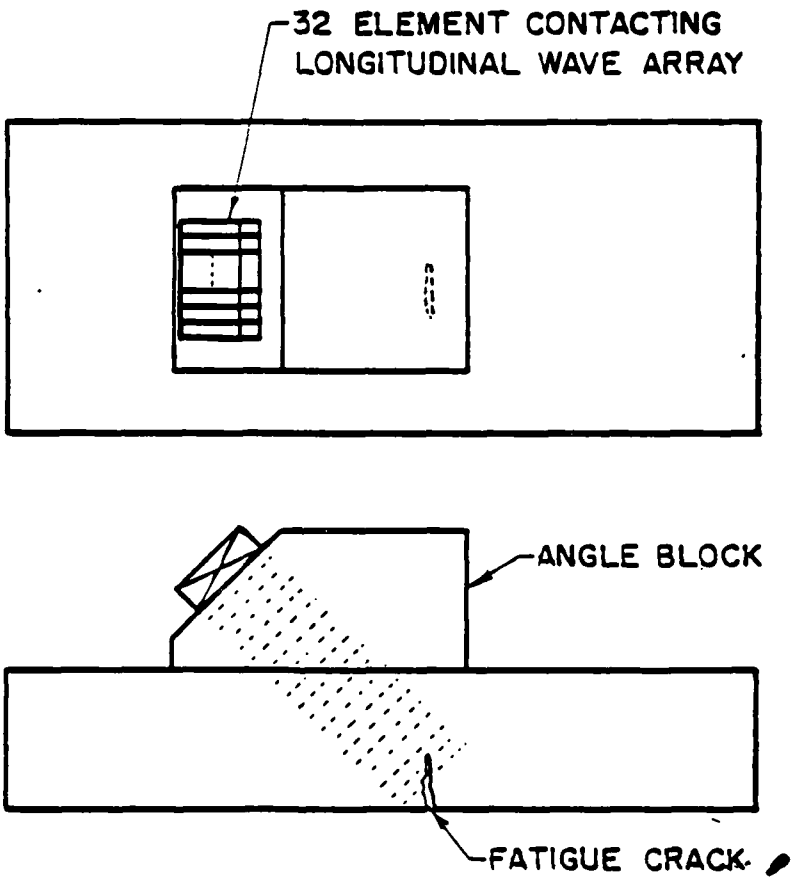

Fig. II.9. Schematic diagram of the imaging experiments with the direct contacting arrays.

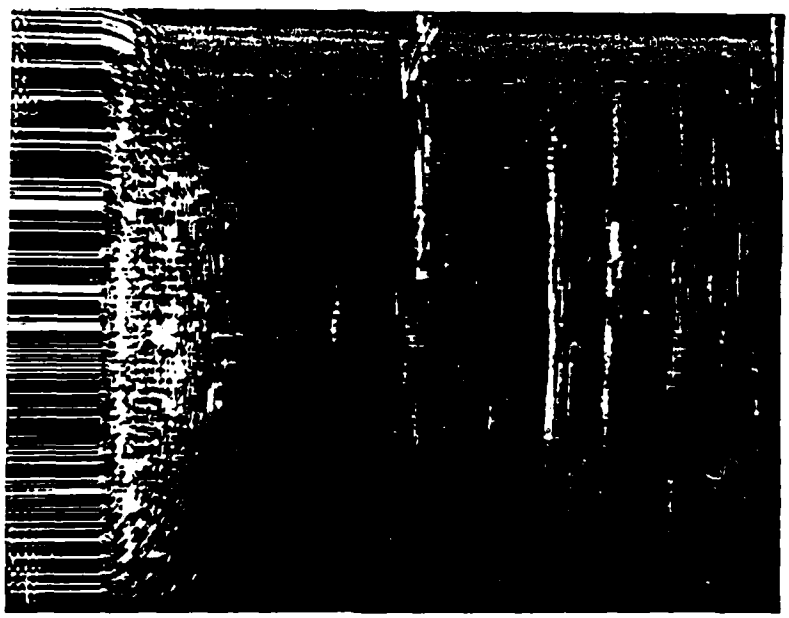

Fig. II.10. Image of the 10 mm fatigue crack using the direct contacting longitudinal array in the geometry shown in Fig. 9.

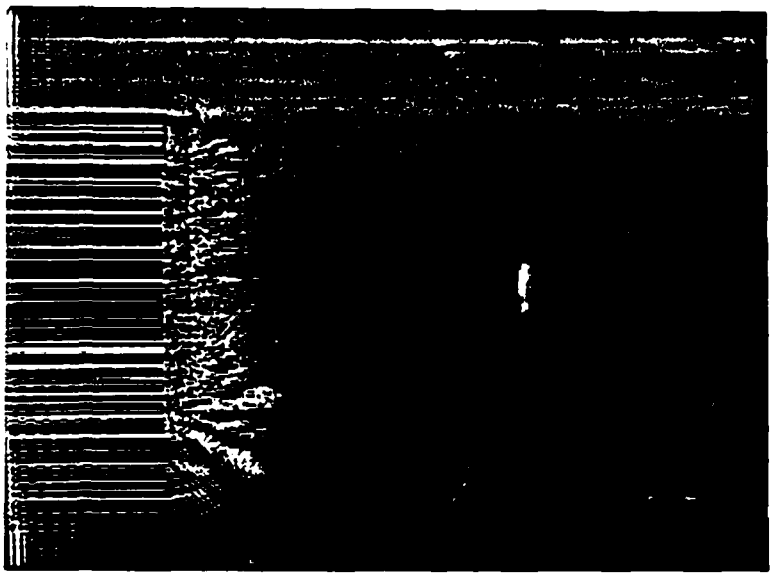

Fig. II.11. Image of the same 10 mm fatigue crack using the direct contacting shear wave array in the same geometry.

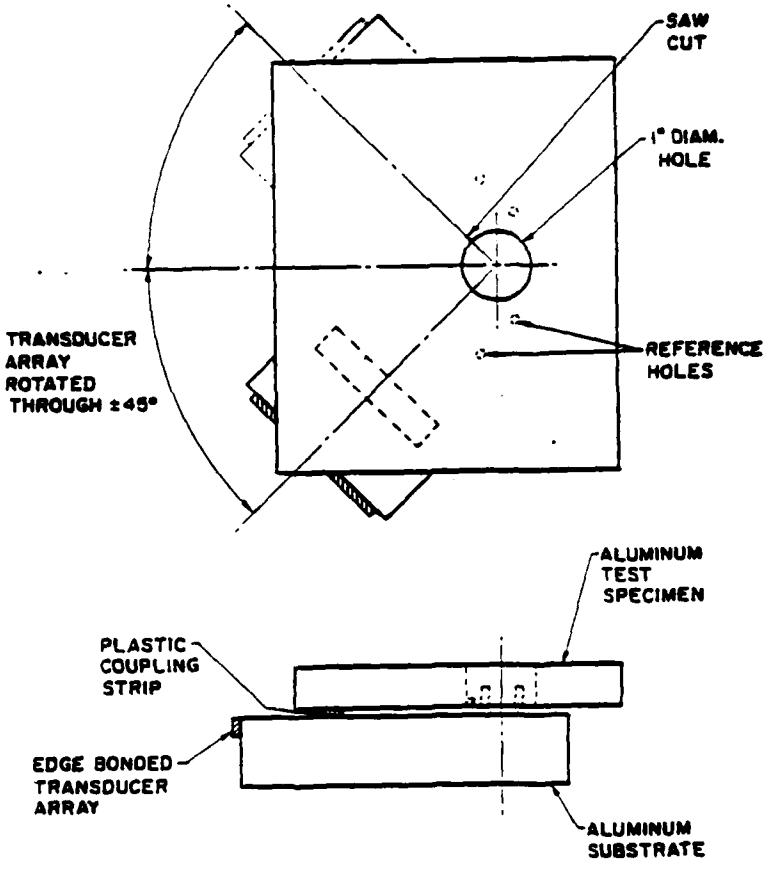

Fig. II.12. Geometry of the composite image experiment. A focused image is obtained from each of seven different viewing angles. The seven viewing angles are spread over 90° at 15° intervals.

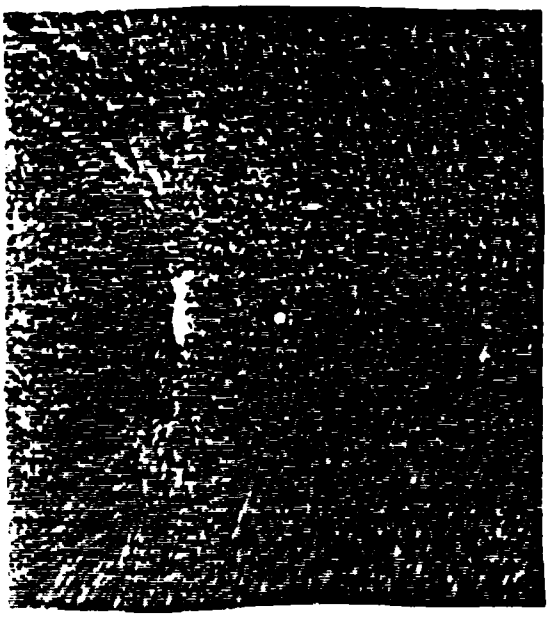

Fig. II.13. A focused image of the hole and SAW cut from a single viewing angle.

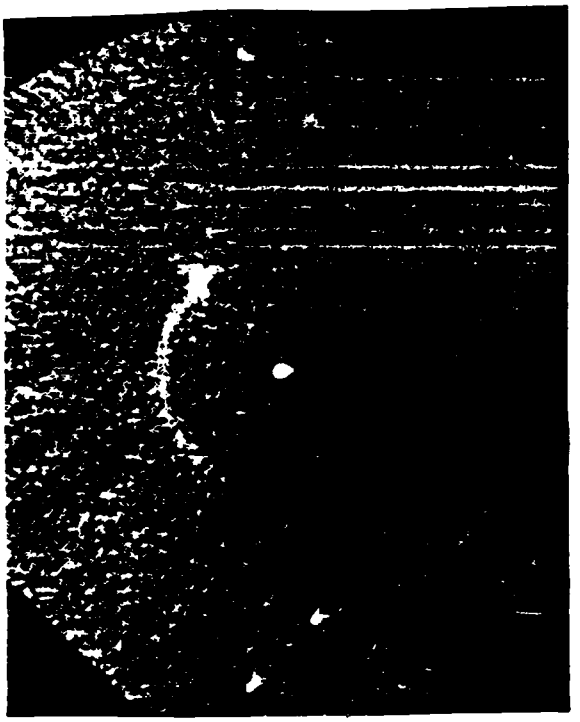

Fig II.14. The composite image obtained by photographically combining the images from seven different angles.

III. STRESS ANALYSIS OF CRACKED ELASTIC SOLIDS

D. M. Barnett, G. Tolf, and G. Wong

1. Introduction

One of the most powerful techniques for performing stress analysis of elastic solids containing stress concentrators such as cracks, involves the solution of integral equations. For a given problem one may formulate any of a number of integral equations capable of producing a solution to the problem at hand. The choice of integral equation to be solved is often a matter of individual taste and the type of data one wishes to extract from such a calculation. At the present time it is not clear which of the many possible integral equations approaches is best to use for a given problem, and this is one of the questions which the present work seeks to address. What does seem to be clear is that if one is only (or primarily) interested in evaluating stress intensity factors, almost any integral equation formulation will suffice.

The motivation for the present work is two-fold. Firstly, there is a need among the Stanford research group, engaged in nondestructive evaluation, to have the in-house capability of performing stress analysis of cracked samples for comparison of theory with stresses measured using acoustic techniques. Secondly, since there is likely to be increased effort at detecting and describing surface cracks (a common occurrence in fatigued samples) using surface wave techniques, theoretical predictions of stresses and displacements, excited when surface waves interact with cracks, are essential for assessing experimental results. It turns out that many previous

numerical studies of the deformation states about edge-cracked solids (even under static loading) have been based on erroneous assumptions, and we felt it necessary, before proceeding to dynamic problems, to reinvestigate static edge crack problems in a more thorough and systematic way. During the past year we have performed such an investigation, and the results of this study are described in what follows.

2. Static Loading of a Half-Space Containing an Edge-Crack

Consider a semi-infinite isotropic linear elastic half-space containing an edge crack of unit length, as shown in Fig. III.1. The most direct method of obtaining an integral equation pertinent to this problem, when the half-space is loaded in far-field tension, is to represent the crack (which is a surface across which the elastic displacement is discontinuous) by a distribution of elementary displacement discontinuities or dislocations. The unknown distribution $f(t)$ is the solution of the following integral equation (in non-dimensional form):

$$\int_0^1 f(t) \left(\frac{1}{x - t} \, dt \right) + K(x,t) = -1; \qquad 0 < x < 1 \qquad (1)$$

This is a singular integral equation due to the presence of the Cauchy kernel $(x - t)^{-1}$; the remaining part of the kernel $K(x,t)$ is non-singular (except at $x = t = 0$), and is algebraic. It is well known that in integral equations of this type, a unique solution is obtained only by specifying something about the behavior of $f(t)$ at the end-points $t = 0$ and $t = 1$. At $t = 1$, the leading edge of the crack, one expects a stress

singularity and it is natural to f to behave as $(1 - t)^{-1/2}$. At $t = 0$, it turns out that one can only require that $f(0)$ be bounded (from physical considerations). Previously, numerical treatments have erred by requiring $f(0)$ to either vanish or obey restrictions which have been motivated by numerical rather than physical considerations. Once Eq. (1) has been correctly solved, one can compute as many features of the deformation field as desired.

Erdogan, Gupta, and Cook[1] have proposed a numerical scheme for solving equations like Eq. (1) by expanding $f(t)$ in Jacobi polynomials, the precise nature of the polynomials being determined by the behavior of $f(t)$ at its endpoints. As stated, the method breaks down due to the semi-definite nature of the end constraint at $t = 0$. The approach we developed during the past year circumvents this difficulty. In essence, we expand the unknown $f(t)$ in a series of Legendre polynomials of the first kind of even order, i.e.,

$$f(t) = \sum_{n=1}^{\infty} \frac{P_{2n}(t)}{(1 - t)^{1/2}} a_n \qquad (2)$$

where a_n are to be determined. This choice is consistent with the end conditions of the problem. As is typical in this class of problems, one decides to solve the integral equation (1) at a finite number (N) of points s_N between 0 and 1, and to truncate the expansion (2) so that instead of solving (1) we solve a linear system of algebraic equations for the unknown a_n. The question remains as to the choice of x_N and the choice of discrete values of t for which the integral in (1) is to be approximated by quadrature. The choice of t's and x_N is termed a collocation procedure, and in the example at hand, the collocation points turn out to be the roots of

$Q_{2N+1}(x) = 0$, where the Q's are Legendre polynomials of the second kind of odd order. The important point to note is that $x = 0$ is a root and this allows one to consistently solve (1) without invoking non-physical assumptions about the behavior of $f(t)$ at $t = 0$.

The importance of the success of the current technique for solving (1) is that, unlike previous numerical solutions of this test problem, it will provide accurate results for the surface displacements on the half-space boundary. The ability to produce reliable surface data will be of extreme importance for future studies of surface wave-edge crack interaction. It is common among investigators of this class of problem to claim success for their numerical methods by comparison of numerically determined stress intensity factors with those found analytically. Using only <u>two</u> collocation points, our method reproduces the known stress intensity factor to better than 1% accuracy, but, of course, the deformation field will not be well represented. This points out that comparison of stress intensity factors is hardly a sensitive and reliable method of assessing the overall utility of a numerical scheme used to solve equations of type (1).

Figure III.2 shows the computed variation of $f(t)$ versus t for numbers of collocation points ranging from $N = 4$ to $N = 48$. There exists a minimum in $f(t)$ near $t = 0$ and this is reflected in the inflection point in the crack opening displacement vs. distance along the crack, depicted in Fig. III.3. The results are part of a manuscript being prepared for submission for publication.

References

1. F. Erdogan, G. Gupta, and T. S. Cook, "Numerical Solution of Singular Integral Equations," Methods of Analysis and Solutions of Crack Problems, Ed. G. C. Sih, Noordhoff (1972).

2. G. Tolf, G. Wong, and D. M. Barnett, "The Edge Crack Revisited," in preparation.

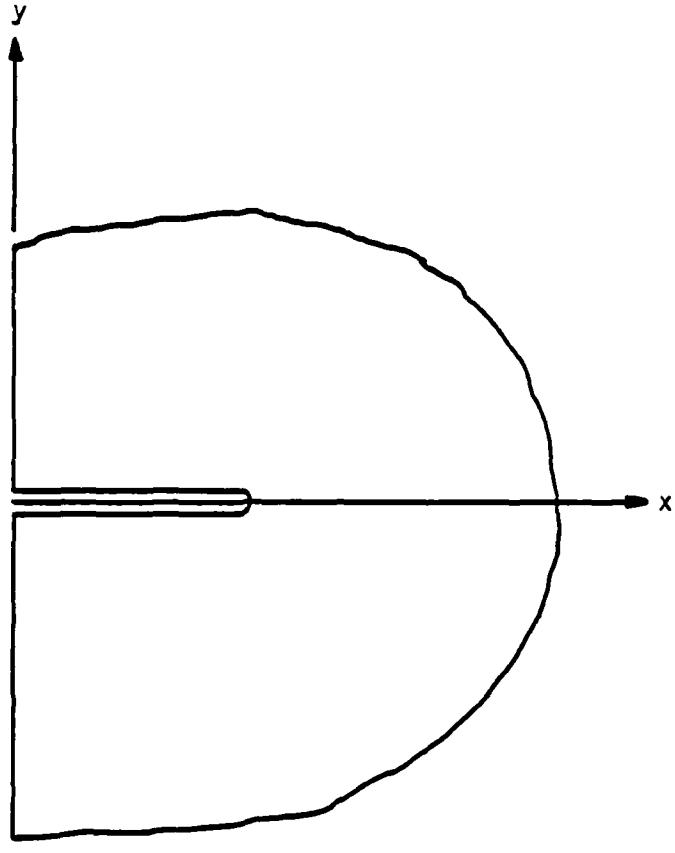

Fig. III.1. An edge crack in a half-space.

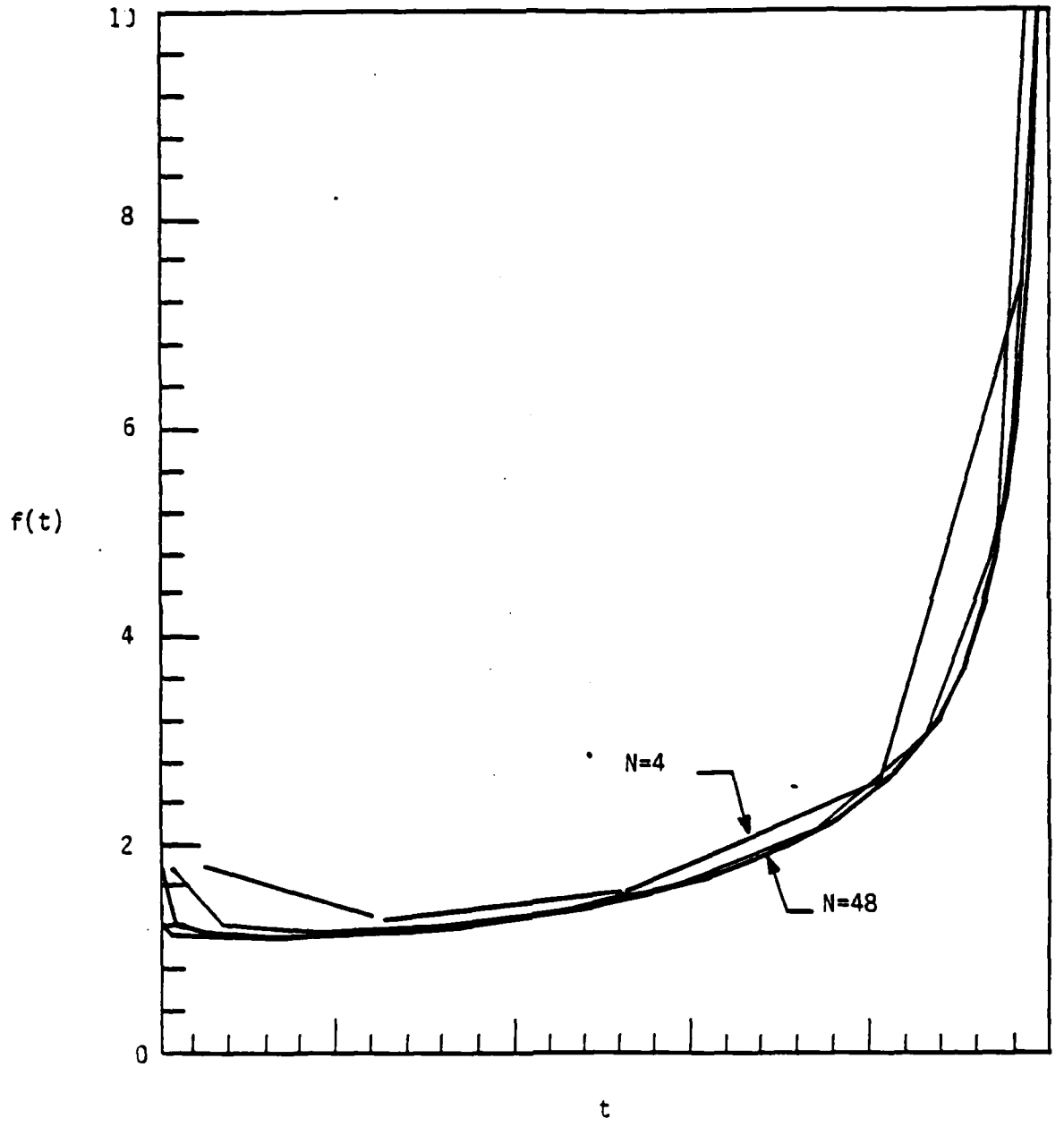

Fig. III.2. f(t), the dist bution function, vs. t.

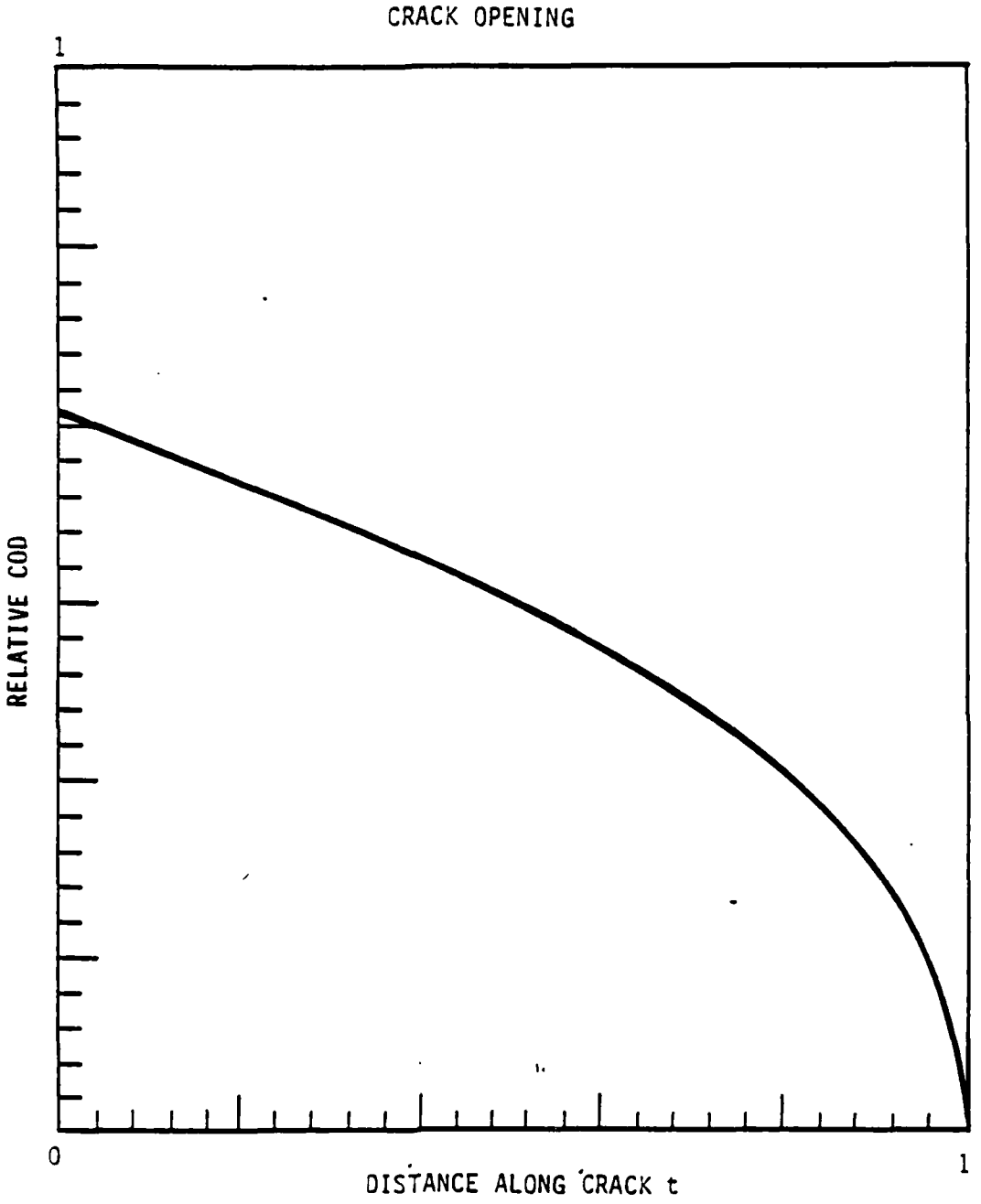

Fig. III.3. Crack opening displacement.

IV. CHARACTERIZATION OF MICROSTRUCTURE

J. Shyne, G. S. Kino, N. Grayeli, S. Bennett, and F. Stanke

1. Introduction

Our work on the acoustic characterization of microstructure has used several different experimental techniques during the period of this report and has required the development of new theoretical methods. These are: (a) attenuation of longitudinal acoustic waves in steel. The three-echo comparison method and apparatus described in earlier reports was entirely satisfactory for these expeirments; (b) Rayleigh wave velocity measurements, thus necessitating the innovation of new equipment and techniques; (c) attenuation in aluminum. This has required an extension of the pulse-echo attenuation measurement method. The higher frequencies required, 50 MHz and higher, have introduced experimental problems not encountered during the lower frequency work with steels; (d) a formal scattering theory is being developed to predict attenuation, velocity change as a function of frequency, grain size, and texture. This has been preceded by a more heuristic scattering theory which takes account of two phase materials and has been used to describe results obtained in carbon steels.

2. Acoustic Attenuation in Steels with Mixed Ferrite-Pearlite Microstructure

Well formulated theories for microstructural attenuation exist only for the simple case of single-phase, polycrystalline materials with uniformly sized, equiaxed grains and apply to frequencies such that $ka \ll 1$ or $ka \gg 1$, where a is the dimension of the average grain, and k is the

wave number, i.e., $2\pi/\lambda$ where λ is the wavelength. Such theories all contain a term that represents the average change in acoustic impedance across grain boundaries caused by elastic anisotropy and random misorientation. We have developed a simple extension of this idea to describe acoustic scattering at grain boundaries and interphase boundaries in a structure consisting of two phases; this includes density discontinuities at boundaries as well as elastic discontinuities. Our two-phase acoustic scattering theory predicts that mixed two-phase microstructures should exhibit greater attenuation than single-phase polycrystalline microstructures consisting entirely of either phase (grain size constant). The maximum in attenuation is predicted to occur with approximately 50/50 volume percents of the two phases, but with more than 50% of the more elastically anisotropic phase.

The acoustic attenuation was measured in a series of plain carbon steels with carbon contents ranging from 0.12 to 0.93 weight percent. These steels were identically heat treated to have mixed pearlite plus ferrite microstructures. Carbon steel was chosen as the specimen material because of the great technological interest in steel and because steel provided a convenient test material. The results are shown in Fig. IV.1.

Ferrite is essentially pure iron. Pearlite is actually a two-phase mixture of ferrite and Fe_3C (cementite). The two phases occur as parallel, alternate, uniform layers. The lamellar layer spacing in pearlite is typically 0.2 to 0.5 μm , about 10^{-3} of the acoustic wavelength at 10 MHz , so a colony of pearlite (a region with constant lamellar spatial orientation) scatters like a homogeneous crystallite or grain, and mixed microstructures consisting of ferrite grains and pearlite colonies scatter

like two-phase mixtures of equi-axed, similar sized grains of two phases, pearlite and ferrite. The volume percent of pearlite varies linearly with carbon content from 0 to 100% pearlite as the carbon content varies from 0 to 0.8 weight percent.

With our set of five steels, the maximum in attenuation occurred near 0.55% carbon, or at about 69 volume percent pearlite. This indicates that pearlite is considerably more anisotropic elastically than ferrite. This is consistent with our observation that the attenuation was higher in the 0.93% C steel (essentially 100% pearlite) than in the 0.12% C steel with 15% pearlite plus 85% ferrite.

The theoretical treatment of acoustic scattering in two-phase microstructures and its experimental confirmation appear to be a significant advancement of acoustic attenuation theory. However, it also suggests the limited utility of such attenuation measurements for microstructural assessment (e.g., the NDE measurement of pearlite content or carbon content of an unknown pearlite steel) because attenuation is a double valued function of the carbon content in pearlitic steels.

3. Prior Austenite Grain Size and Attenuation in Steel

Other workers have reported that acoustic attenuation in steel is influenced by the prior austenite grain size. Quantitative data demonstrating this assertion are scarce. When steel is heat treated, it is heated to a temperature of 750° to 1300°C where the austenite phase is stable. During cooling to room temperature, the austenite transforms to pearlite and ferrite (slow cooling) or to martensite (fast cooling). The grain size of the

austenite prior to transformation into pearlite or martensite depends upon the austenitizing temperature, the higher the temperature, the larger the grain size. The higher the austenitizing temperature is (and thus with larger prior austenite grains), the greater is the acoustic attenuation.

We have investigated this phenomenon by measuring the attenuation of longitudinal acoustic waves in specimens of AISI 4140 steel austenitized at temperatures ranging from 900°C to 1200°C and either slow cooled or oil quenched. The attenuation in the pearlitic specimen increased by a factor of 10 times as the austenitizing temperature was raised; the martensitic specimens showed a similar but smaller, 5 times, increase from lowest to highest austenitizing temperature. For both the pearlitic and martensitic specimens, the greatest change in attenuation occurred between specimens austenitized at 100° and 1100°C . This is consistent with the expected behavior of the "fine grained" steels; virtually all commercial alloy steels contain a small amount of aluminum nitride that inhibits austenite grain growth below about 1100°C . Since the pearlitic and martensitic specimens austenitized at identical temperatures must have had identical austenite grain size, the larger attenuation change in pearlite suggests a change in either pearlite or martensite anisotropy, depending on austenite grain size.

The austenite grain size effect is very strong. Apparently the pearlite and the martensite that forms from any given austenite grain inherits its crystal orientation from the austenite, so that each transformed prior austenite grain continues to act as an acoustic scattering center because of the inherited elastic anisotropy of the pearlite or martensite, even though that volume now consists of many pearlite colonies and martensite platelets.

This work is not complete. It remains to measure the prior austenite grain sizes metallographically, and to analyze the attenuation coefficients and grain sizes using theories for stochastic and Rayleigh grain scattering, and to correlate attenuation and velocity variations in these specimens.

4. Surface Microstructure Characterization by SAW

There are many situations where the surface properties of materials are of paramount importance. Some examples are carburized steel, peened parts, plated objects, and induction-hardened steel. Surface acoustic waves (SAW), or Rayleigh waves, offer the means for characterizing selectively and nondestructively the near-surface regions of the samples being measured. The displacement amplitude of a surface acoustic wave falls off rapidly with distance below the surface, and the effective depth is approximately equal to the wavelength. Thus, the depth of the surface region sampled by SAW methods can be adjusted by choosing appropriate frequencies, thereby changing the effective depth of the acoustic waves.

The selectivity of surface waves for sampling surface properties has been quite apparent for years; several authors[1,2] have discussed the potential of SAW NDE methods. However, little relevant experimental effort has been reported.

We have been experimenting with samples of AISI 4615 steel, a low carbon, carburizing grade of alloy steel. Flat plate specimens have been carburized to depths of 0, 0.7, 1.1, and 2.0 mm . These specimens make a useful set for investigating SAW effects because the range of surface layer depths corresponds to Rayleigh waves of convenient frequencies, and we expect that

acoustic velocity will vary by about 1% within the carburized surface layer because of the gradient of carbon content from the surface (about 1.0 percent weight carbon) to the interior (0.15 percent weight carbon). This should make Rayleigh waves dispersive in the frequency range where the penetration depth of the wave varies from extending well beyond the surface layer into the bulk to being entirely confined to the surface layer.

The acoustic system illustrated in Fig. IV.2 has been used to measure the phase shift of Rayleigh waves propagating on the test specimens. The source frequency is varied under computer control in small steps from 2 to 6 MHz, so that the coherently detected and filtered output voltage V varies cyclically. Tone bursts of the carrier frequency are applied to a wedge transducer that launches Rayleigh waves on the test specimen surface. A similar, pick-up transducer is used to receive the signal after transmission over a known, fixed distance (1"). We determine the variation in phase ϕ that arises from the perturbation of the Rayleigh wave velocity by the surface layer. For that reason measurements are made on the uncarburized specimen to provide a reference data set; any changes in phase for that specimen are due to phase shifts in the electronics and transducers. Even in the absence of any dispersion there is a large, linear phase shift as the frequency is varied, and this tends to obscure the smaller, frequency-dependent variations caused by a surface layer. The reference data set is used to separate out not only unwanted electronic phase shifts but also the basic linear phase shift as the frequency is varied. Typical results are shown in Fig. IV.3. Clearly there are differences dependent on the carburized layer thickness.

We are now developing iterative methods based on the Laplace transform and adaptive matching to trial profiles to provide carburized layer depth and carbon content from measurements of this type. Transducer characteristics are important in SAW experiments on surface layers. The limited bandwidth of the wedge transducers limits the practical range of operating frequency. We intend to build new transducers operating up to perhaps 10 MHz . For very thin surface layers still higher frequencies will be required, and this must involve a different transduction method since wedge transducers of the type currently being used are not practical above 10 MHz . We hope to make use of the fiber optic probe for this purpose. This is described in Section VI.

5. Assessment of Aluminum Alloy Heat Treatment by Acoustic Attenuation Measureme:

High strength aluminum alloys, e.g., 2024 and 7075 alloys, achieve maximum strength by age hardening. In such alloys, the heat treatment consists of solution treatment to put the maximum amount of solutes into solid solution, followed by aging at room temperature or slightly elevated temperatures, 125 to 150°C , to permit the precipitation of Cu, $MgSi_2$ or other submicroscopic particles. We have attempted to follow the aging process in 6061 aluminum by measuring the change in acoustic attenuation with time.

The low acoustic attenuation in aluminum has required attenuation measurements at rather high frequencies in order for the attenuation to be high enough for any precision. For that reason, we have made measurements with a polyvinylfluoride transducer operating at 40 to 50 MHz . At these high frequencies certain peculiarities have occurred that have thus far prevented accurate attenuation measurements by our three-echo comparison

method. This technique required careful orientation of the transducer relative to the specimen for maximum front and back face echo amplitudes. Oddly, the front and back face echoes from our aluminum specimens are not maximized at the same transducer orientation. Either the specimen aluminum is inhomogeneously anisotropic or the high-frequency transducer has introduced some acoustic or instrumentational perturbation. Work is continuing to get the "bugs" out of the technique so that the study of aluminum heat treatment can be pursued using both acoustic velocity and attenuation measurements.

6. Theory of Attenuation and Velocity Change Due to Grain Size and Texture

The theories for scattering of acoustic waves from grains only take account of scattering from equi-axed grains, neglecting texture effects and predict only attenuation effects, not the change in velocity due to grain size. Furthermore, these theories typically are evaluated only in two regimes, the low-frequency range where they predict an f^4 variation in attenuation and the high-frequency range where they predict an f^2 variation in attenuation. Therefore, it is not possible to determine the distribution of grain sizes by acoustic measurements, using the presently-available theories.

We have thus felt that it is necessary to reformulate the theory to take account of the attenuation and velocity changes over the whole frequency range so that we can use the measurements to determine the distribution of grain size, textural effects, and the connection between anisotropy in the velocity measurements as a function of angle and the texture of the material. To do this we have started with perhaps the best theory available at the present

time, the Russian theory of Lifshits and Parkomovski,[4] and are making considerable use of yet another Russian source, the book Wave Propagation in a Random Medium, by Chernov.[3] We are also basing our ideas on an earlier grain scattering theory for porous ceramics, performed by Evans, Tittmann, Ahlberg, Khuri-Yakub, and Kino,[5] which gave accurate experimental results.

The Lifshits theory takes account of scattering by using a Born approximation regarding an individual crystallite as a small perturbation in a uniform medium consisting of crystals with the average elastic constants. Then it calculates an additional term corresponding to the perturbation of the field at one point in an individual crystallite by the fields generated by scattering from other points in the same crystallite. In this theory, $C_{IJ}(\theta,\phi,\psi)$ is the elastic constant of an individual crystallite rotated through the Euler angles θ,ϕ,ψ from its position when the crystal axes are lined up along the coordinate axes. It is necessary to calculate the quantities $\langle C_{IJ}\rangle$ and $\langle C_{IJ}^2\rangle - \langle C_{IJ}\rangle^2$. In the high and low-frequency limits, considerable simplifications can be made, but this is not so easy if one wishes to take account of texture or the attenuation variation over the whole frequency range.

We have made considerable progress with the procedures required. To carry out these averages, it is necessary to find the rotated elastic constant by multiplying a set of seven matrices together. A major simplification for cubic crystals is to write $C_{IJ}(\theta,\phi,\psi)$ in the form

$$C_{IJ}(\theta,\phi,\psi) = C_{IJ}^0 + \alpha_{IJ}(\theta,\phi,\psi)\,(C_{11}^0 - C_{12}^0 - 2C_{44}^0)^2 \qquad (3)$$

where C^0_{IJ} is the corresponding elastic constant in a set of coordinates referred to the crystal axes, and $\alpha_{IJ}(\theta,\phi,\psi)$ is the quantity we need to determine before averaging. It is apparent, for simplicity, that if we put $C^0_{11} = 0$, $C^0_{44} = 0$, we can still determine α_{IJ} and thus determine the elastic constant for a general rotation of a cubic crystal. Similar simplifications are possible for hexagonal crystals.

The second simplification we have made in our approach to the theory is to construct, on an HP 85 computer, an algebraic program for multiplying the simplified set of matrices required together. This makes it possible to evaluate the individual terms required when multiplying the 6×6 matrices together. In fact, we have determined that because of symmetry, we only need to find six separate terms. We have followed this procedure through, and where the results can be checked with the literature, they agree. We are now in a position to use these results in the Green's function formalism we have developed to predict attenuation and velocity changes as a function of the grain parameters. We will first make these predictions for equiaxed grains and check our results experimentally. In particular, we will formulate the theory in terms of the distribution of grain sizes, the intention being to arrive at simplified measurement techniques for the distribution of grain sizes using a video-camera and a Fourier transform approach to find the spatial frequencies occurring in the distribution rather than counting sizes by eye. Our plan is then to go on and take account of texture effects, the change in velocity with texture, and grain size. Such results have not been available in the literature before.

References

1. B. R. Tittmann, G. A. Alers, R. B. Thompson, and R. A. Young, "Characterization of Subsurface Anomalies by Elastic Surface Wave Dispersion," 1974 Ultrasonics Symposium, Proceedings.
2. H. Hirao, M. Kyukawa, H. Toda, and H. Fukuoka, "Rayleigh Wave Propagation in Media with Work Hardened Surface Layers," Private Communication, September, 1980.
3. L. A. Chernov, Wave Propagation in a Random Medium," McGraw-Hill Book Company, Inc., New York (1960).
4. M. Lifshits and G. D. Parkhomovski, J. Exp. Theoret. Phys, Vol. 20, No. 2, pp. 175-182 (1950).
5. A. G. Evans, B. R. Tittmann, L. Ahlberg, B. T. Khuri-Yakub, and G. S. Kino, J. Appl. Phys., 49 (51) or is this page no? (1978)

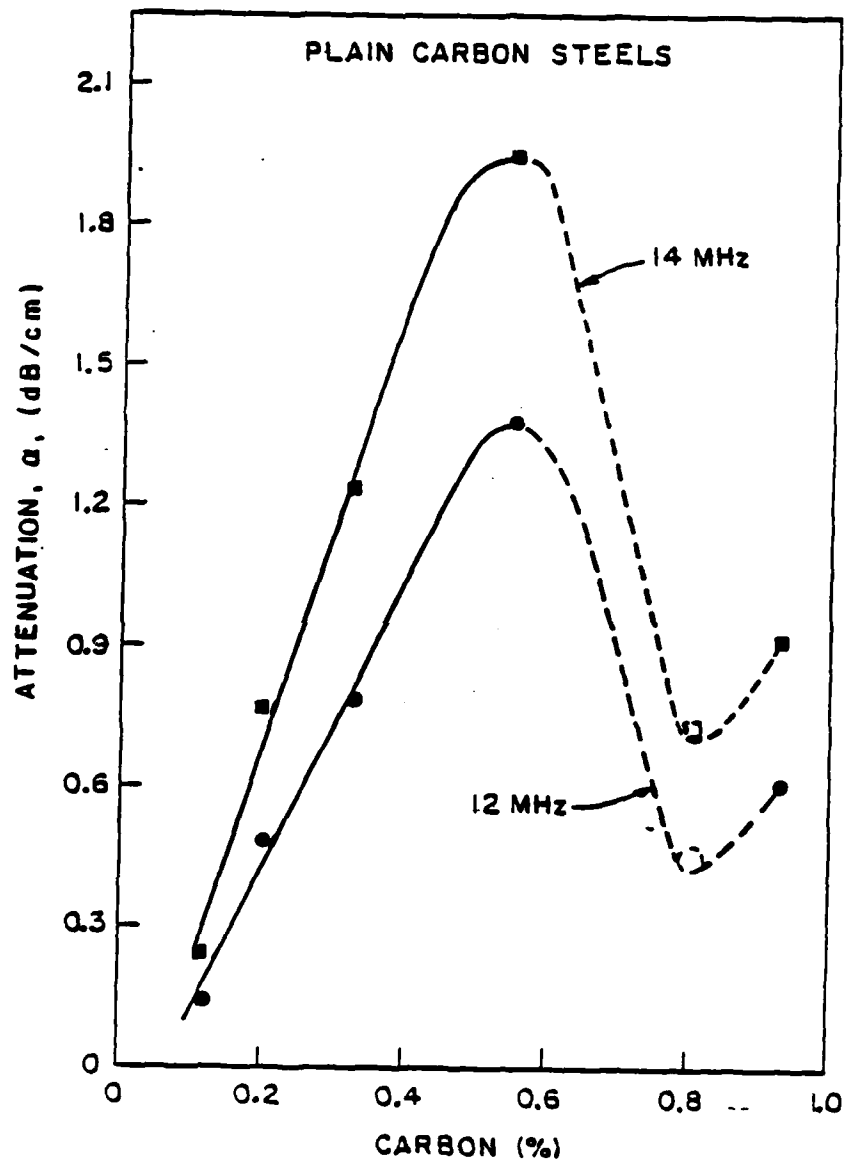

Fig. IV. 1. Attenuation versus weight percent carbon with a maximum at 0.55 percent carbon at two frequencies.

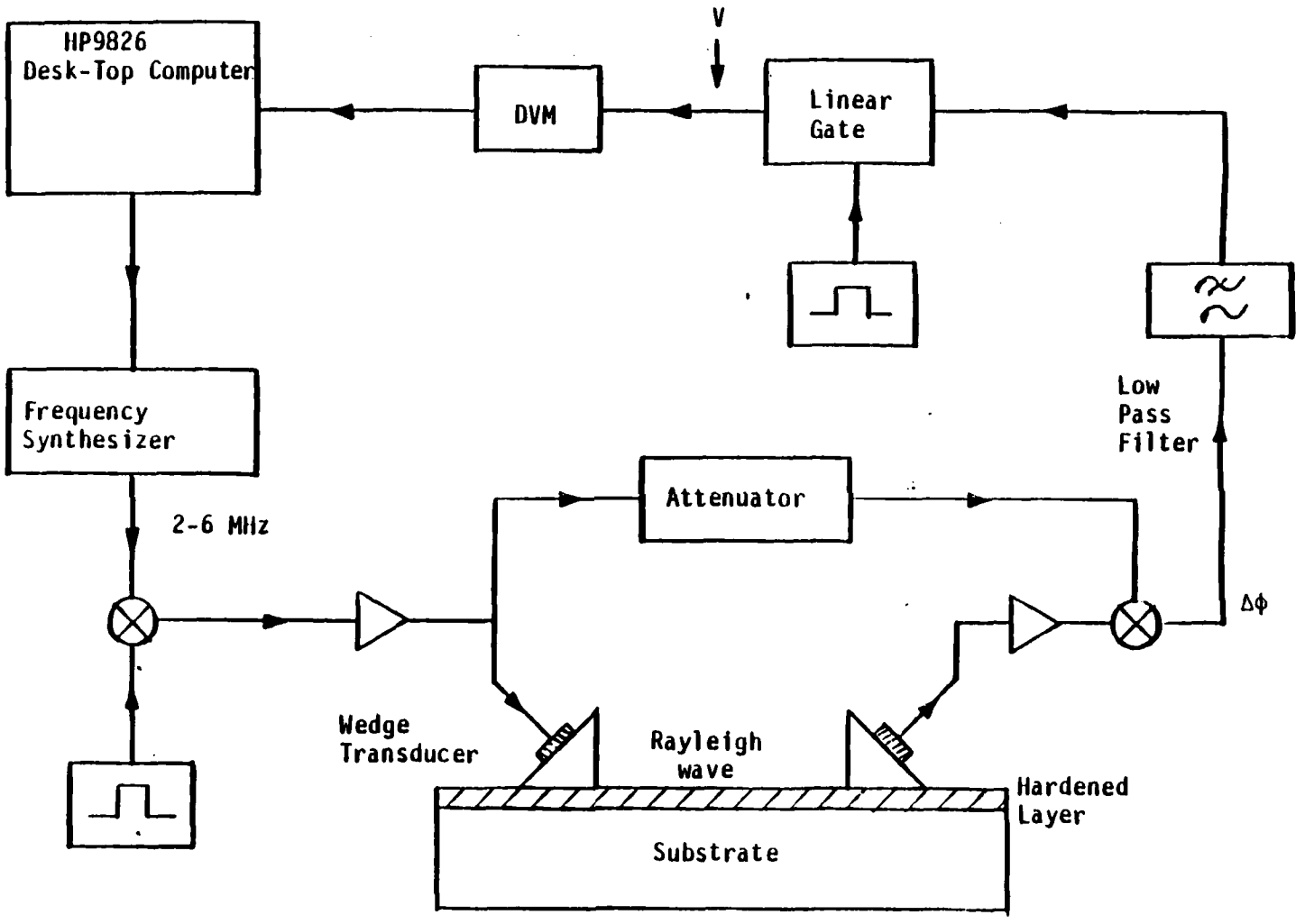

Fig. IV.2. Acoustic instrumentation system for measuring the velocity dispersion of Rayleigh waves caused by carburized surface layers.

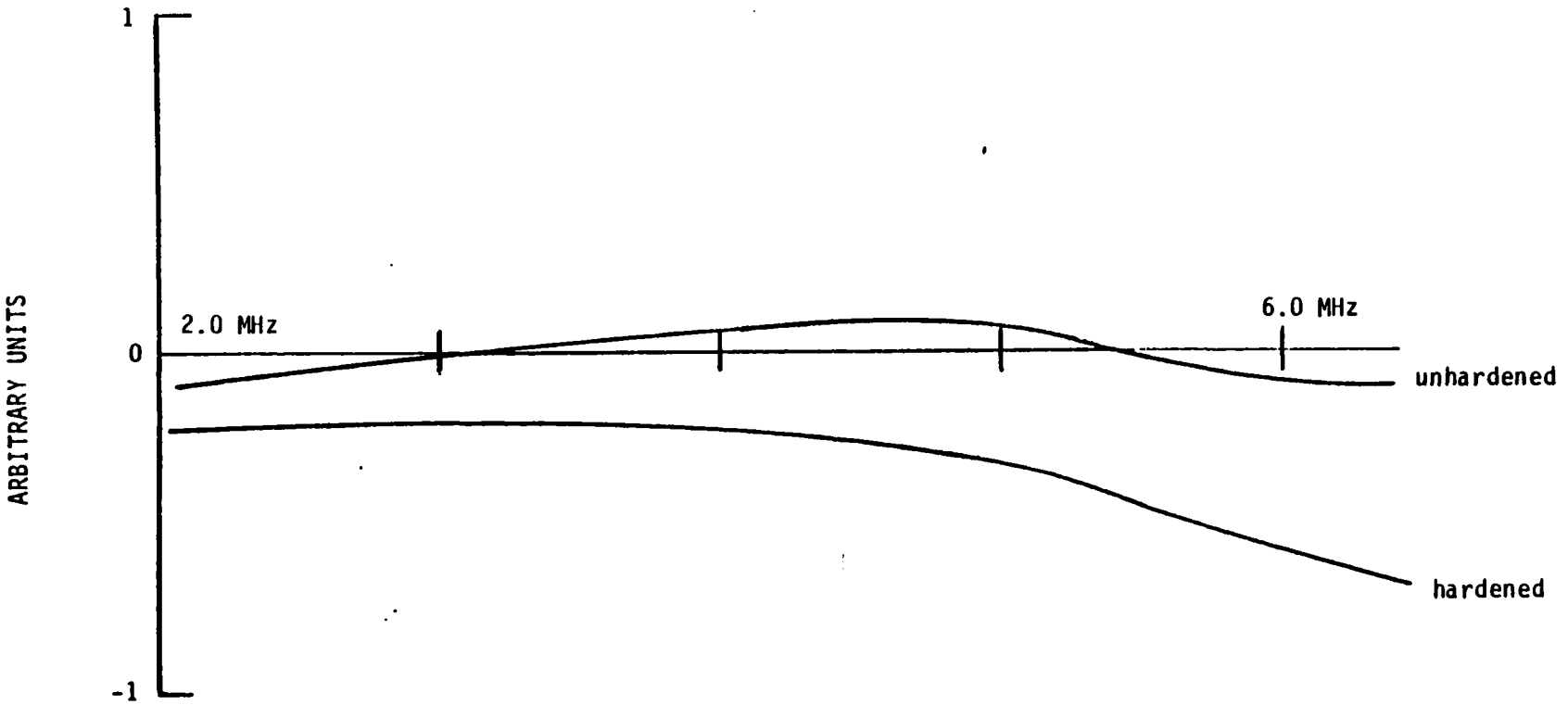

Fig. IV. 3. Experimental comparison of SAW phase shift for hardened and unhardened steel samples.

V. ENERGY INTEGRALS

G. Herrmann, A. Herrmann, and M. Fisher

1. Introduction

During the period reported, further significant progress has been made in the area of quantitative nondestructive characterization of stress fields around cracks. This obviously is an important problem area, aiming at increasing our predictive capabilities.

As is widely recognized, the relevant quantities governing the behavior of cracks in stressed bodies are the so-called stress intensity factors and energy release rates. The latter may also be termed generalized forces acting on cracks and can be related to so-called conservation integrals. Knowing stress intensity factors implies knowing how much below critical values the structural element is loaded and thus what safety factors there exist for crack growth. Ultimately, we hope that we will be able to predict crack skewing effects based on these energy integrals. So far, only the J integral has received much attention by others. It is obvious, however, that to describe skewing, energy integrals which take account of rotation must be used. These effects are associated with the so-called L integral.

The basic concept of conservation integrals and energy release rates has been discussed in its fundamentals in the previous Annual Scientific Report (dated November, 1980), and for this reason will not be further reviewed here. Suffice it to recall that three different types of integrals are known to exist, namely the J, L and M integrals. In three dimensions the J integral is a three-dimensional vector, as is L, while M is always a

scalar. In two dimensions, the J integral is a two-dimensional vector, while the L integral then has only one non-vanishing component.

2. Experimental Results

One phase of the work during the period reported emphasized the determination of conservation integrals, and thus of stress intensity factors in plane specimens containing a plane crack subjected to mixed-mode loading. In one study the path-independent L integral has been determined. It was first shown theoretically that it may be interpreted as the energy release rate for rotation of either the crack with respect to the applied stress field, or the converse. It is further shown theoretically that the L integral depends not only on the elastic properties of the sample, the crack length and the stress intensity factors in Mode I and Mode II, but also on the applied normal stress in the direction parallel to the crack.

In one experiment, the energy release rate was determined directly from compliance measurements. Comparison with theoretical predictions showed that indeed the L integral could be determined in this manner. In another series of experiments, both the J integral (more precisely the component parallel to the crack) and the L integral have been determined experimentally in a nondestructive fashion using ultrasonic measurements with longitudinal waves. The experiment involved a plane specimen with a slanted central crack subjected to tension. The method used in determining the conservation integrals from ultrasonic measurements has been itself developed under the current project and has been termed the "rescaling" technique. Since both the L and the J integrals involve, as mentioned, the two stress intensity

factors for Mode I and Mode II loading, the latter can be calculated from a measurement of the former. Comparison of the results obtained experimentally showed good agreement with theoretically calculated values.

If the force applies to a specimen containing a crack grow large, then plastic zones will develop in regions of high stress concentration, i.e., near crack tips. The methodology selected to study this problem requires these plastic regions not to be too large, such that the scanned region contains a sufficiently large elastic part, while still being suitably distant from the boundaries of the specimen. Such an experiment has been carried out successfully, showing that the numerically-obtained values, using finite element calculations, come quite close to the acoustically-determined quantities.

All of the above experiments were carried out using longitudinal waves only. A more complete determination of the stress field would be possible if, in addition, measurements with shear waves could be made. While longitudinal waves give information (for plane stress) on the value of the principal stress, measurements with shear waves would give the values essentially of the difference of the principal stresses.

3. Shear Wave Measurements

Scanning with a shear transducer is obviously more difficult than with a longitudinal transducer because contact with the specimen must be established. During the last year, considerable effort has been spent in improving the techniques of scanning with shear wave transducers. The PZT shear transducers used previously had a very short fatigue life, and in order

to increase it, a stiff backing between the PZT and flexible rubber was thought to be beneficial. Different materials and arrangements were tried. The final design of the transducer had a fairly long life (~1000 cycles), but eventually the silver epoxy, which is quite brittle, cracked under the cyclic loading.

Lapped Epoxy Backing

We went back to an epoxy resin with the V140 and LP-3 hardeners and lapped the surface of a cured epoxy plug, again using the thin film bond to attach the PZT. There was still a problem with the electrical connection, and when we drilled a hole through the epoxy and attached a gold wire, the PZT once again broke at the stress concentration after repeated loadings.

We tried using a number of different types of PZT, including PZT8 and PZT5H and found that, with our backings, the PZT-5H gave the best results. We also tried a number of different self-aligning techniques, including a small pneumatically operated brass bellows and rubber of different thicknesses.

Final Design

This combined a number of the ideas we tried. A 5/8" diameter 1/4" long plug with a flattened cone shape on one end (see Fig. V.1) is cast on a one part epoxy resin, one part Versamide V140 and 0.5 parts Thiokol LP-3 epoxy mixture, and cured at ~100^{0}C for 24 hours. A small hole is drilled through the plug at a point on the edge of the 1/4" diameter flattened top and a small indentation is cut out of the flat surface starting at the hole. A copper wire is then placed in the back side of the hole and the hole and indentation are both filled with silver epoxy.

After the silver epoxy has cured, the flat top surface (both epoxy mixture and silver epoxy) is lapped to a 15 μm finish. The surface is then thoroughly cleaned, as is the metallized PZT-5H chip (7 x 100 x 200 mils). A thin film bond is made, as described above, joining the PZT to the flat, lapped surface. Because of the silver epoxy, which is bonded to part of the PZT, there is now an electrical connection between the back of the PZT and the copper wire, but since the PZT is bonded to a flat lapped surface, there is no stress concentration. The epoxy plug is now glued to a piece of 1/8" thick rubber which is attached to a bakelite and brass transducer base which fits into a holder on the stress rig. The copper wire runs through the rubber backing and through the backelite into the base, where it is soldered to a coaxial cable attachment.

The measured insertion loss of the new transducer is -15.5 dB with a 70 lb contact force into 1 cm thick aluminum and -20.3 dB with a 30 lb force, which is substantially better than any of the other transducers tested. It has a center frequency of 6.8 MHz into aluminum, and a clean impulse response with very little ringing. No cracks have formed under repeated loading and the front face has worn very evenly.

At the time of writing, the only normal-incidence contact shear transducer commercially available is made by Panametrics. This transducer, which has a front wear plate, has a measured insertion loss of -51 dB into a 1 cm thick aluminum plate. As in the other cases, this measurement was made without a shear couplant with a 70 lb contact force. However, because this transducer has a larger area than the ones we built, the actual pressure was somewhat lower than used in the other tests. Even with a shear couplant,

the insertion loss was -26 dB , almost 75% higher than ours was without the couplant.

Although our new design has been quite successful, there is still some room for improvement. We are considering the use of a heavier metallization on the front face of the PZT, so that it will wear for a longer time, and intend to investigate further the question of self-alignment. One possibility is to attach a rubber ring around the PZT which would contact the sample along with the PZT and give a greater self-aligning moment to the epoxy plug.

References

1. A. G. Herrmann, "On Conservation Laws of Continuum Mechanics," Int. J. Solids, Structures, Vol. 17, 1981, pgs. 1-9.
2. A. G. Herrmann, "Variational Formulations in Defect Mechanics: Cracks and Dislocations," Acta Metallurgica, in print.
3. A. G. Herrmann and G. Herrmann, "On Energy-Release Rates for a Plane Crack," J. Appl. Mech., in print.
4. A. G. Herrmann and G. Herrmann, "Energy Release Rates for a Plane Crack Subjected to General Loading and Their Relation to Stress-Intensity Factors," Proceedings of the ARPA-AFML Conf. on NDE, July 1980, in print.
5. R. B. King, G. Herrmann, and G. S. Kino, "Use of Stress Measurements with Ultrasonics for Nondestructive Evaluation of the J Integral," Eng. Fracture Mech., in print.
6. R. B. King and G. Herrmann, "Nondestructive Evaluation of the J and M

Integrals," J. Appl. Mech., Vol. 48, 1981, pgs. 83-87.

7. R. B. King and G. Herrmann, "Acoustoelastic Determination of Forces on a Crack in Mixed-Mode Loading," submitted for publication.

8. R. King and G. Herrmann, "Evaluation of the L Integral in a Cracked Specimen Using Compliance Measurements," submitted for publication.

9. R. B. King and G. Herrmann, "Application of Ultrasonic Stress Measurements to Nondestructive Evaluation of the J Integral in Elastic-Plastic Deformation," submitted for publication.

TOP VIEW AND CUTAWAY VIEW

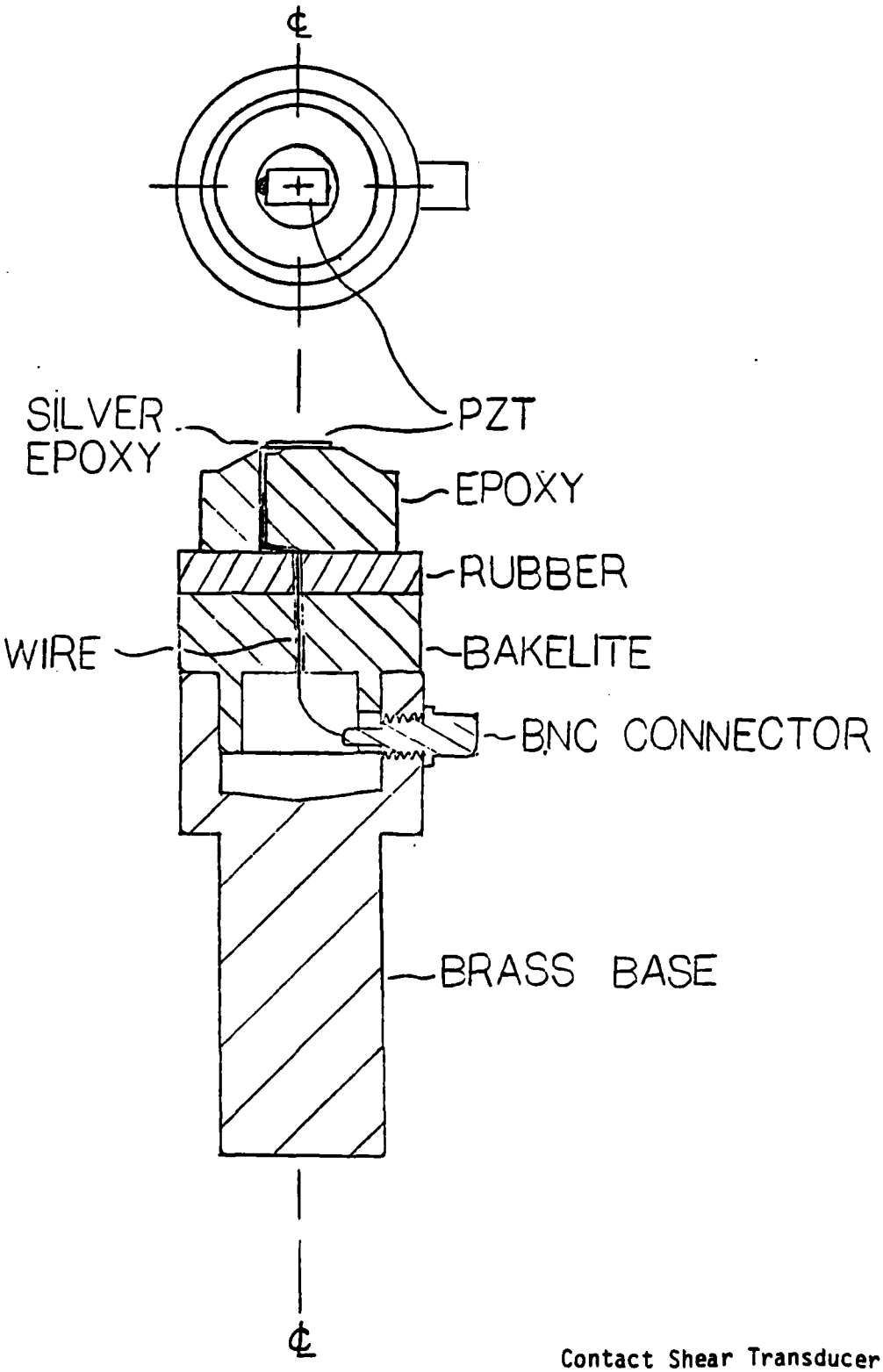

Contact Shear Transducer

VI. FIBER-OPTIC ACOUSTIC PROBING SYSTEM

G. S. Kino, J. E. Bowers, R. Jungerman, and S. D. Bennett

A new technique for probing acoustic waves on a metal surface has been investigated for use as a facility for the laboratory. Therefore, this particular project has been financed in part out of several contracts, including the AFOSR contract.

The aim of this method is to use the reflection of a laser beam from a metal surface as a probe. If this metal surface is excited by an acoustic wave, then the reflected laser beam will be phase-modulated by the acoustic wave. In the past, techniques have been worked out by Ash and his co-workers for such probing, which eliminate the effect of vibrations. We have duplicated their system using a He-Ne laser source and have obtained good success in probing acoustic surface waves on $LiNbO_3$, ceramic and metal surfaces.

Our aim is to probe acoustic waves in NDT applications, where the material being investigated is not necessarily on an optical bench, and might even be a considerable distance from the optical bench. Examples might be a sample being stressed in a tensile test rig, or a large engine part which would not be convenient to place on an optical bench. Therefore it was our aim to use a fiber-optic link so that we could carry out probing in a remote position.

We have constructed a new single-mode fiber-optic link for this purpose, using technology developed by H. J. Shaw and his co-workers in this laboratory. In particular, we have used their single-mode fiber directional

coupler. The fiber-optic system we have constructed works well and it has already been used to give an approximately 5 μm resolution on the surface of the sample. We have investigated scattering from machined surfaces, lapped surfaces, and highly polished surfaces and have found that, at least with machined surfaces, the light loss on reflection back into the exciting fiber is only of the order of a few dB .

Our aim in the end is to use this technique as a remote probe. Some examples for possible use are for constructing synthetic aperture images of flaws excited by acoustic waves, or to look at near-field effects due to scattering from cracks. We believe this will give us another technique for determining the depth of a crack where the fringing fields from low-frequency waves incident on the crack might be expected to extend to a distance associated with the depth of the crack.

At the present time, in agreement with AFOSR and AFML, the work has been transferred to an AFML contract. Instead, synthetic aperture high-frequency imaging experiments at frequencies greater than 5 MHz will be carried out on this contract.


FILMED
8